Interactive Power Oscillation and Its Suppression Strategy for VSG-DSG Paralleled System in Islanded Microgrid*

Zhiyong Yuan[1], *Xia Shen*[2*], *Yingjie Tan*[1], *Zhenhua Tan*[2] *and Jinyong Lei*[1]

(1. Electric Power Research Institute, CSG, Guangzhou 510663, China;
2. National Electrical Energy Conversion and Control Engineering Technology Research Center, Hunan University, Changsha 410082, China)

Abstract: A virtual synchronous generator (VSG) can provide inertial support through renewables and energy storage. It generally operates in parallel with a diesel generator (DSG) in an islanded microgrid. However, unforeseen interactive power oscillations occur in the paralleled system when loads fluctuate. These may also burn out the VSG owing to its low overcurrent capacity. The mechanism and suppression strategy of the power oscillation of a VSG-DSG paralleled system are investigated. It reveals that the interactive power oscillation is caused essentially by the physical difference and parameter mismatch between the VSG and DSG. Then, the elimination condition of oscillation generation is derived. Subsequently, a comprehensive suppression control strategy based on virtual inductance and dynamic mutual damping technology is proposed. Finally, the experimental results verify the effectiveness of the proposed method.

Keywords: Islanded microgrid, VSG-DSG paralleled system, oscillation mechanism, virtual inductance, dynamic mutual damping, suppression strategy

1 Introduction

Distributed energy resources are generally integrated into the microgrid through power electronic converters. The virtual synchronous generator (VSG) is being regarded as a type of grid-friendly grid-connected converter. This is because it can replicate characteristics of conventional synchronous generators (SGs) and provide certain inertial support to the vulnerable microgrid [1-2].

In the existing microgrid projects, diesel generators (DSGs) continue to be employed as important power supply units to ensure the stability and safety of islanded microgrids. Hence, VSGs generally need to operate in parallel with DSGs. However, because they differ in physical structures, control principles, and parameters [3], large power oscillations are generated within the paralleled system when loads fluctuate. It degrades the power supply quality and may even exceed the thermal current limitation of the power electronic device-based VSG [4-5].

Many investigations have been performed on the operation characteristics of a standalone VSG or paralleled VSG system in a microgrid. In Refs. [6-8], the small-signal model of VSG was established to optimize the control parameters according to the optimal damping ratio. Thereafter, a higher response speed and smaller power overshoot could be obtained. In Ref. [9], the concept of adaptive virtual inertia of VSG was presented to realize the suppression of power oscillation. Although this method can achieve good performance when loads fluctuate, the introduction of a differential unit would amplify the influence of the high-frequency components. In Ref. [10], the virtual impedance was designed effectively for a paralleled VSG system to address the power oscillation issue. Subsequently, Ref. [11] also concluded that the essential mechanism of the power oscillation phenomenon of paralleled VSGs is based on the undesirable instantaneous active power sharing between these.

The aforementioned studies were aimed mainly at a standalone or paralleled VSG system consisting of

Manuscript received January 20, 2021; revised July 24, 2021; accepted September 14, 2021. Date of publication December 31, 2022; date of current version December 31, 2021.
* Corresponding Author, E-mail: shenxia@hnu.edu.cn
* Supported by the Science and Technology Project of China Southern Power Grid (ZBKJXM20180211).
Digital Object Identifier: 10.23919/CJEE.2022.000043

pure power electronic devices. It differs from an inverter and synchronous generator-based DSG paralleled system. Ref. [12] demonstrated that a VSG-DSG paralleled system could straightforwardly become unstable under large load fluctuations or fault conditions. In Ref. [13], the output power of a current-controlled inverter is regulated according to the instantaneous detected frequency to suppress the power oscillation issue when it is paralleled with a DSG. Ref. [14] investigated the dynamics of the VSG-DSG paralleled system. In addition, an active power reference generation strategy for VSG was proposed to suppress the power oscillation. However, the essential mechanism of the dynamic process has not been analyzed. In Ref. [15], the inertia and output impedance of the VSG are designed as large to be as those of the DSG in advance to solve the oscillation problems under paralleled operation. However, the performance under normal conditions was compromised. In particular, owing to the manufacturing and measurement deviations, it is difficult to fully equalize VSG-DSG by parameter design. A marginal error may result in other severe issues. In Ref. [16], a damping power control unit was introduced to the control system of a VSG. It generates the compensation power based on the difference between the rated frequency and DSG frequency to help attenuate the power oscillation.

To summarize, the mechanism of interactive power oscillation of VSG-DSG paralleled systems during load fluctuations is unclear. Moreover, the existing suppression control methods mostly directly increase the inertia and impedance parameters of VSGs to damp the oscillation [17-19]. However, this is at the expense of certain important dynamic performance.

To address the above issues, this study first analyzes the mechanism and suppression conditions of power oscillation in a VSG-DSG paralleled system. It is revealed that the oscillation is caused essentially by the physical difference and parameter mismatch between the VSG and DSG. Thereafter, a power oscillation suppression strategy based on the virtual inductance and dynamic mutual damping is proposed. It does not affect their steady-state operations.

The remainder of this paper is organized as follows: Section 2 analyzes the mechanism and elimination condition of power oscillation of the VSG-DSG paralleled system. Section 3 elaborates the proposed strategy. The experimental verifications are presented in Section 4. This is followed by the conclusions in Section 5.

2 Mechanism of power oscillation in VSG-DSG paralleled system

2.1 VSG-DSG paralleled system

The topology and control structure of the VSG-DSG paralleled system is shown in Fig. 1. A DSG is powered by a diesel engine and connected to the microgrid through an SG. The prime mover is regulated by the speed governor to maintain the balance between the input and output torques [12]. The excitation system provides DC excitation for the SG to maintain the stability of the terminal voltage of the DSG. Meanwhile, a VSG is an inverter that replicates external characteristics of a conventional SG, which is highly controllable and flexible.

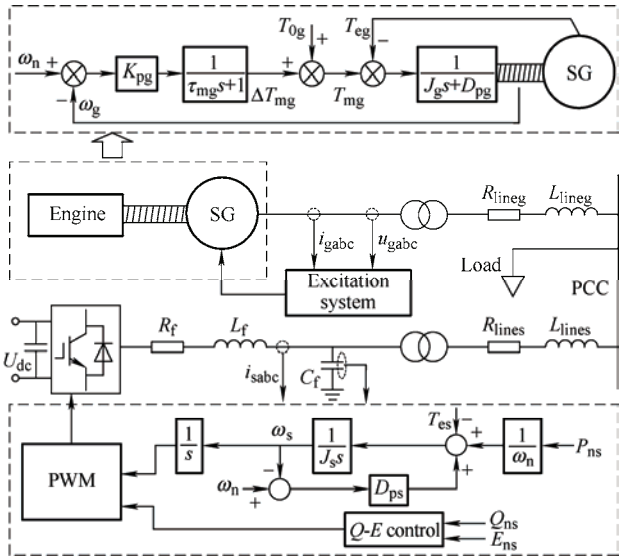

Fig. 1 Paralleled VSG-DSG system in islanded microgrid

In Fig. 1, the swing equation of VSG is [2, 12]

$$J_s\dot{\omega}_s = T_{ms} - T_{es} - D_{ps}(\omega_s - \omega_n) \tag{1}$$

where, J_s, D_{ps}, ω_n, ω_s, T_{ms}, and T_{es} are the virtual inertia, damping coefficient, rated/detected angular frequencies, virtual mechanical torque, and electromagnetic torque, respectively, of the VSG.

The swing equation of the DSG system [12, 19] is

$$\begin{cases} J_g\dot{\omega}_g = T_{mg} - T_{eg} - D_{pg}\omega_g \\ \tau_{mg}\dot{T}_{mg} = T_{0g} - K_{pg}(\omega_g - \omega_n) - T_{mg} \end{cases} \tag{2}$$

where J_g, ω_g, D_{pg}, T_{mg}, and T_{eg} are the inertia, angular frequency, damping coefficient, mechanical input torque, and electromagnetic output torque, respectively, of the DSG. K_{pg} and τ_{mg} are the control parameter and time constant, respectively, of the speed governor.

It is evident that the VSG and DSG differ in physical structure and control parameters. For example, the VSG does not have the mechanical speed governor of the DSG. Therefore, their dynamics differ, and active power oscillation of the parallel system would occur when there are loads and other external fluctuations.

2.2 Mechanism of power oscillation between VSG and DSG

The power oscillation mechanism is analyzed in this section by establishing the small-signal model of the VSG-DSG paralleled system. The equivalent circuit is shown in Fig. 2.

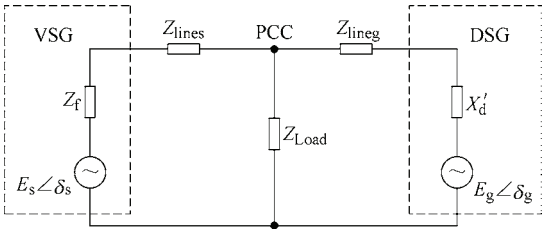

Fig. 2 Topology of paralleled VSG-DSG system

where $E_s\angle\delta_s$ and $E_g\angle\delta_g$ are the output voltages of the VSG and DSG, respectively. Z_f, Z_{lines}, and Z_{lineg} are the output filter impedance of the VSG, line impedance between VSG and the point of common coupling (PCC), and that between DSG and PCC, respectively. X'_d is the *d*-axis reactance of the DSG. For convenient explanation, the variables of VSG and DSG are represented by the subscripts "s" and "g", respectively. Then, the equivalent output impedances Z_{os} and Z_{og} of the VSG and DSG can be expressed as

$$\begin{cases} Z_{os} = Z_f + Z_{lines} = R_{os} + jX_{os} \\ Z_{og} = X'_d + Z_{lineg} = R_{og} + jX_{og} \end{cases} \tag{3}$$

Considering that Z_{os} is mainly inductive, the active power transferred from the VSG to the PCC can be expressed as

$$P_s = 3\frac{E_sE_{PCC}(R_{os}\cos\delta_s + X_{os}\sin\delta_s) - R_{os}E_{PCC}^2}{R_{os}^2+X_{os}^2} \approx 3\frac{E_sE_{PCC}(R_{os} + X_{os}\delta_s) - R_{os}E_{PCC}^2}{R_{os}^2+X_{os}^2} \tag{4}$$

Similarly, the output power of the DSG can be expressed as

$$P_g \approx 3\frac{E_gE_{PCC}(R_{og} + X_{og}\delta_g) - R_{og}E_{PCC}^2}{R_{og}^2+X_{og}^2} \tag{5}$$

The power loss of resistance can be expressed as

$$P_{Ros} = \frac{P_s^2+Q_s^2}{E_s^2}R_{os} \quad P_{Rog} = \frac{P_g^2+Q_g^2}{E_g^2}R_{og} \tag{6}$$

Then, the power balance equation is

$$P_s + P_g - P_{Ros} - P_{Rog} = P_{Load} \tag{7}$$

Subsequently, the state space model of the paralleled system is constructed, and disturbance separation and linearization are carried out to obtain [20]

$$\begin{cases} \Delta\dot{x} = A\Delta x + B\Delta u \\ \Delta y = C\Delta x + D\Delta u \end{cases} \tag{8}$$

where

$$x = [\Delta\omega_s \ \ \Delta\omega_g \ \ \Delta T_{mg} \ \ \Delta\delta_s]^T \tag{9}$$

$$u = \left[\Delta P_{ns} \quad \Delta P_{ng} \quad \Delta P_{Load}\right]^T \tag{10}$$

The system stability can be estimated by the system matrix

$$\boldsymbol{A} = \begin{bmatrix} -\frac{D_{ps}}{J_s} & 0 & 0 & -\frac{3G_1}{J_s\omega_n} \\ 0 & -\frac{D_{pg}}{J_g} & \frac{1}{J_g} & -\frac{3G_2(G_3G_1 - G_1)}{J_g\omega_n(G_2 - G_4G_2)} \\ 0 & -\frac{K_{pg}}{\tau_{mg}} & -\frac{1}{\tau_{mg}} & 0 \\ \frac{1}{1-\left(\frac{G_3G_1 - G_1}{G_2 - G_4G_2}\right)} & \frac{-1}{1-\left(\frac{G_3G_1 - G_1}{G_2 - G_4G_2}\right)} & 0 & 0 \end{bmatrix} \tag{11}$$

where G_1-G_4 represent the intermediate variables.

$$\begin{cases} G_1 = \dfrac{E_s E_{PCC} X_{os}}{R_{os}^2 + X_{os}^2} \quad G_2 = \dfrac{E_g E_{PCC} X_{og}}{R_{og}^2 + X_{og}^2} \\ G_3 = \dfrac{6R_{os}}{E_s^2} \dfrac{E_s E_{PCC}(R_{os} + X_{os}\delta_s) - R_{os} E_{PCC}^2}{R_{os}^2 + X_{os}^2} \\ G_4 = \dfrac{6R_{og}}{E_g^2} \dfrac{E_g E_{PCC}(R_{og} + X_{og}\delta_g) - R_{og} E_{PCC}^2}{R_{og}^2 + X_{og}^2} \end{cases} \tag{12}$$

Then, the system characteristic equation can be Eq. (13)

$$\begin{aligned} \left|\lambda E - A\right| = & \frac{3G_1(G_2 - G_4G_2)}{J_s\omega_n(G_2 - G_4G_2 - G_3G_1 + G_1)} \times \\ & \left(\frac{K_{pg}}{J_g\tau_{mg}} + (s + \frac{D_{pg}}{J_g})(s + \frac{1}{\tau_{mg}})\right) - \\ & \left(s + \frac{D_{ps}}{J_s}\right)\left(s + \frac{1}{\tau_{mg}}\right)\frac{3G_2\left(G_3G_1 - G_1\right)}{G_2 - G_4G_2 - G_3G_1 + G_1}\frac{1}{J_g\omega_n} + \\ & (s + \frac{D_{ps}}{J_s})(s + \frac{D_{pg}}{J_g})(s + \frac{1}{\tau_{mg}})s + (s + \frac{D_{ps}}{J_s})\frac{K_{pg}}{\tau_{mg}}\frac{1}{J_g}s \end{aligned} \tag{13}$$

The active power time constants of the VSG and DSG are represented by Eq. (14) [2]. In general, time constant τ_{VSG} can be altered according to the capacity and frequency fluctuation limitation of the VSG. Meanwhile, τ_{DSG} is a fixed value and determined by the physical structure of the DSG [2]

$$\tau_{VSG} = \frac{J_s}{D_{ps}} \quad \tau_{DSG} = \frac{J_g}{D_{pg}} \tag{14}$$

Subsequently, for convenient analysis, two scenarios are considered according to the grade difference between the active power time constants of the VSG and DSG: $\tau_{DSG} \gg \tau_{VSG}$, and $\tau_{DSG} \approx \tau_{VSG}$ or $\tau_{DSG} \ll \tau_{VSG}$. Accordingly, the solution of Eq. (13) can be divided into the two scenarios to investigate the influence of the physical difference and control parameters on the power oscillation of the paralleled system.

2.2.1 Scenario I: $\tau_{DSG} \gg \tau_{VSG}$

In this scenario, Eq. (13) can be simplified as

$$s(s + \frac{1}{\tau_{mg}})\left[s^2 + \frac{D_{ps}s}{J_s} + \frac{3G_1(G_2 - G_4G_2)}{J_s\omega_n(G_2 - G_4G_2 - G_3G_1 + G_1)}\right] = 0 \tag{15}$$

The characteristic equation has three non-zero solutions. One of these is

$$s_1 = -\frac{1}{\tau_{mg}} \tag{16}$$

This negative real root is related to parameters of the speed governor of the DSG. That is, in this scenario, τ_{mg} would cause the system to be in an over-damping state without instability or power oscillations. The other two non-zero solutions can be identified by the delta criterion

$$\Delta = \frac{1}{\tau_{VSG}^2} - \frac{12G_1(G_2 - G_4G_2)}{J_s\omega_n(G_2 - G_4G_2 - G_3G_1 + G_1)} \tag{17}$$

According to the Vieta theorem, Eq. (15) has two real solutions when $\Delta \geqslant 0$. These are located in the negative half axis of the real axis.

When $\Delta < 0$, the other two solutions are

$$s_{2,3} = -\frac{1}{2\tau_{VSG}} \pm \frac{\sqrt{-\Delta}}{2}j \tag{18}$$

At this point, the solution of the power angle of VSG can be expressed as

$$\Delta\delta_s = A_0 \exp\left(-\beta t\right)\cos(\omega_d t + \theta_0) \tag{19}$$

$$\omega_d = \frac{\sqrt{-\Delta}}{2} \quad \beta = \frac{D_{ps}}{2J_s} \quad \theta_0 = \arccos\left[\frac{D_{ps}}{2}\sqrt{\frac{\omega_n J_s(R_{os}^2 + X_{os}^2)}{E_s E_{PCC} X_{os}}}\right] \tag{20}$$

where A_0, ω_d, β, and θ_0 are the amplitude, angular frequency, decay coefficient, and initial phase, respectively, of the power angle.

Combining with Eq. (4), the output power of VSG is

$$\Delta P_s = \frac{3E_s E_{PCC} X_{os}}{R_{os}^2 + X_{os}^2}\Delta\delta_s \tag{21}$$

It can be determined from Eqs. (19)-(21) that when the active power time constant of the DSG is significantly larger than that of the VSG, the system power oscillation is affected mainly by the parameters of the VSG and the line impedance. Meanwhile, the parameters of the DSG have negligible influence. The specific rules are as follows: when the load fluctuates, the power oscillation of the VSG is a sine function whose amplitude decays gradually. When J_s and D_{ps} are smaller, ω_d would be larger. Thereby, the power oscillation frequency would be larger. When D_{ps} is smaller, J_s would be larger and β would be smaller. Thereby, the decay speed of the power oscillation would be lower. In addition, the various impedances mainly affect ω_d, implying that they mainly affect the oscillation frequency.

2.2.2 Scenario II: $\tau_{DSG} \approx \tau_{VSG}$ or $\tau_{DSG} << \tau_{VSG}$

It is difficult to simplify Eq. (13) in this scenario. It is a quartic equation with four roots. The analytical solutions are highly complex. Furthermore, it is difficult to determine the relationship between solutions and parameters intuitively. Therefore, the influence of parameters such as J_s, D_{ps}, J_g, D_{pg}, X_x, K_{pg}, and τ_{mg} on the oscillation would be investigated by the root locus directly.

The eigenvalue distributions when the key parameters vary are shown in Fig. 3. In general, it can be determined that in this scenario, all their parameters and equivalent impedance would have substantial influence on the paralleled system oscillation. In particular, the influence of the speed governor of the DSG is more significant. The specific rules are as follows.

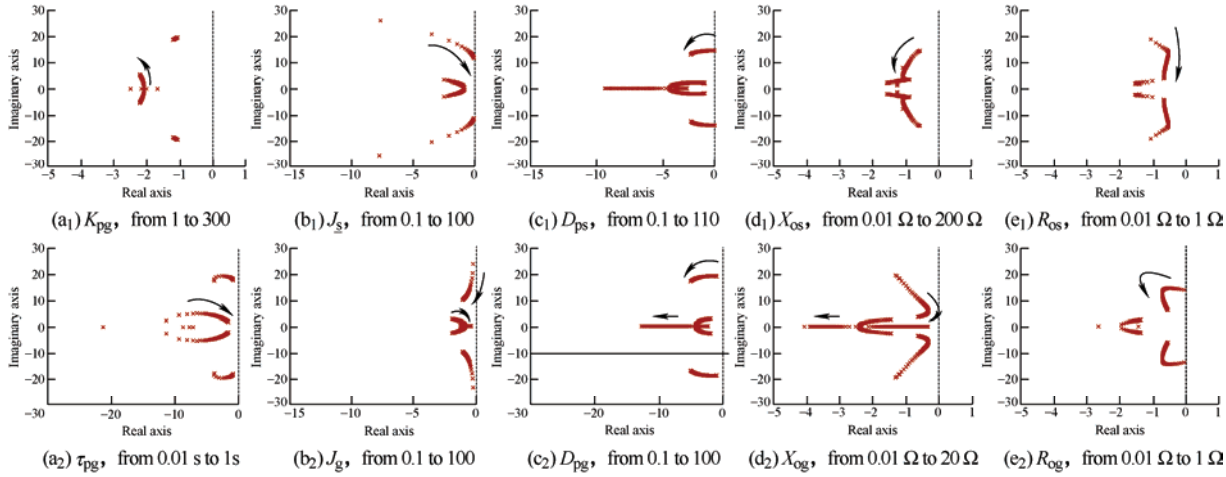

Fig. 3 System eigenvalue distribution when key parameters vary under Scenario II

As shown in Figs. $3a_1$ and $3a_2$, with the increase in τ_{mg}, the system eigenvalues shift closer to the imaginary axis, and the oscillation decay speed would reduce. Meanwhile, with the increase in K_{pg}, the eigenvalues shift away from the negative real axis. This indicates that the oscillation frequency increases.

In Figs. $3b_1$ and $3b_2$, with the increase in J_s, the eigenvalues gradually shift closer to the imaginary axis, and the decay speed and frequency of oscillation would reduce. Meanwhile, the increase in J_g only causes the eigenvalues to gradually shift closer to the negative real axis. That is, J_g has a higher impact on the oscillation frequency rather than the decay speed.

In Figs. $3c_1$ and $3c_2$, with the increase in D_{ps} or D_{pg}, the eigenvalues gradually shift away from the imaginary axis, and the decay speed increases continuously. When these increase to a certain extent, the system would enter the overdamping state.

In Figs. $3d_1$, $3d_2$, $3e_1$, and $3e_2$, with the increase in X_{os} or R_{os} and R_{og} or X_{og}, the eigenvalues continue to shift closer to the negative real axis. It shows that these mainly affect the frequency of power oscillation, which is similar to Scenario I.

The above influence analysis of parameters on the system eigenvalues reveals that the power oscillations in the VSG-DSG paralleled system are caused essentially by the physical difference and parameter mismatch between the VSG and DSG. When the inertia of the DSG is significantly higher than that of the VSG (because D_{ps} is determined by the rated capacity of the VSG, τ_{VSG} is essentially related to J_s), the paralleled system is sensitive only to the parameters of the VSG rather than the DSG. When the inertia of the DSG is similar or significantly smaller than that of the VSG, the system is sensitive to all parameters and is more likely to oscillate. Meanwhile, the impedance further influences the power oscillation frequency in all the scenarios. Certain conclusions are summarized in Tab. 1 for a comprehensive description of the influence of key parameters on the oscillation.

Tab. 1 Influence of control and physical circuit parameters on frequency and decay speed of power oscillation

	Frequency of oscillation	Decay speed of oscillation
Influence parameters	J_s, K_{pg}, J_g, X_{os}, R_{os}, R_{og}, X_{og}	J_s, D_{ps}, D_{pg}, τ_{mg}

2.3 Elimination condition of power oscillation

Several solutions can be considered to suppress the power oscillation in the VSG-DSG paralleled system. ① Replicate the speed governor of the DSG in the VSG controller, and adjust the parameters to completely equalize the mathematical models of the VSG and DSG. ② Reduce the virtual inertia and increase the damping of the VSG. ③ Explore the reasonable condition for the elimination of power oscillation, and optimize the dynamics matching design of VSG and DSG.

Nevertheless, with regard to the first solution, the additional model of the speed governor would impact the dynamics of the VSG. Meanwhile, it is challenging to accurately equate the mathematical models of the VSG and DSG, owing to practical errors. Similar to the above analysis in Scenario II, marginal differences between these are more likely to deteriorate the parallel operation issues. Meanwhile, the second solution would not achieve the original objective, which is to provide inertial support to the microgrid to address the problems such as high frequency ripples.

Therefore, from the perspective of the third solution, the elimination conditions of power oscillation generation are derived directly from the response characteristics of the VSG and DSG in this study. Specifically, to prevent the oscillation, it is necessary to maintain the angular frequency ω and acceleration $\dot{\omega}$ of the VSG and DSG equal before or after the load fluctuations. Combining Eqs. (1), (2), (4), and (5), we can obtain Eq. (22)

$$\frac{\dot{\omega}_{\mathrm{s}}}{\dot{\omega}_{\mathrm{g}}}=\frac{\Delta T_{\mathrm{es}}}{J_{\mathrm{s}}}\Big/\frac{\Delta T_{\mathrm{eg}}}{J_{\mathrm{g}}}\approx\frac{\Delta P_{\mathrm{s}}}{\omega_{\mathrm{n}}J_{\mathrm{s}}}\Big/\frac{\Delta P_{\mathrm{g}}}{\omega_{\mathrm{n}}J_{\mathrm{g}}}=\frac{E_{\mathrm{s}}}{E_{\mathrm{g}}}\cdot\frac{J_{\mathrm{g}}}{J_{\mathrm{s}}}\cdot\frac{X_{\mathrm{og}}}{X_{\mathrm{os}}} \tag{22}$$

Hence, if $\omega_{\mathrm{s}}=\omega_{\mathrm{g}}$ and $\dot{\omega}_{\mathrm{s}}=\dot{\omega}_{\mathrm{g}}$ during the transient process,

$$\begin{cases}E_{\mathrm{s}}=E_{\mathrm{g}}\\ J_{\mathrm{s}}X_{\mathrm{os}}=J_{\mathrm{g}}X_{\mathrm{og}}\end{cases} \tag{23}$$

As shown in Eq. (23), the generation conditions of oscillation can be eliminated if the equivalent impedance and inertia of the VSG and DSG are designed to be inversely proportional and their voltage amplitude are maintained equal. Although there are unalterable differences in their physical structure, oscillation can be suppressed by optimizing controllers of the VSG.

3 Power oscillation suppression control strategy with virtual inductance and dynamic mutual damping

Based on the above analysis, a power oscillation suppression method for the VSG-DSG paralleled system with virtual inductance and dynamic mutual damping technology is proposed. First, the virtual inductance is designed and added to the VSG's controller to satisfy the elimination condition of Eq. (23). Second, the frequency information of the DSG is transferred to the VSG to construct the virtual mutual damping and thereafter, to suppress the instantaneous overshoot and increase the decay speed of oscillation. The proposed strategy is illustrated in Fig. 4. This is followed by a detailed introduction of the operation principle and design considerations.

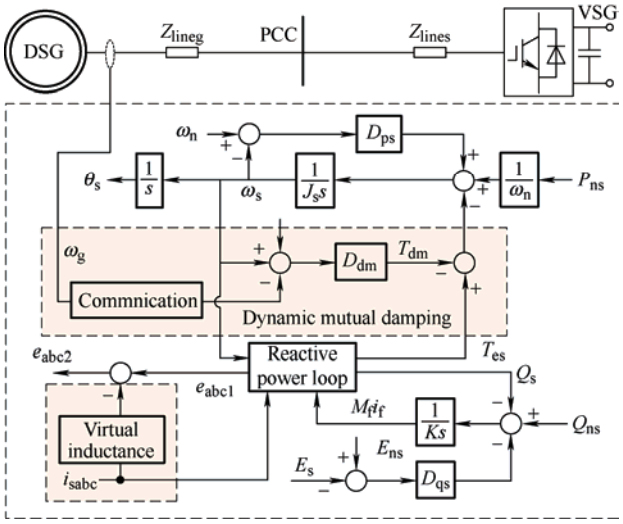

Fig. 4 Proposed overall control strategy for VSG

3.1 Oscillation generation suppression principle with virtual inductance

The block diagram of virtual inductance is shown in Fig. 5. Here, e_{abc1}, e_{abc2}, and i_{sabc} are the initial output voltage, modified voltage reference, and current of the VSG. e_{α}, e_{β}, i_{α}, and i_{β} are the corresponding values in the stationary coordinates. L_{vr} is the virtual inductance.

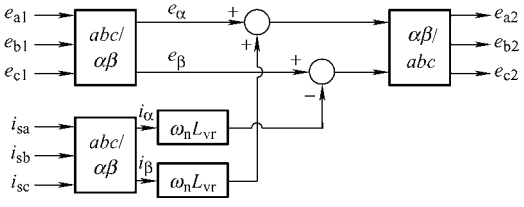

Fig. 5 Block diagram of virtual inductance

As shown in Fig. 5, the virtual inductance L_{vr} is multiplied by the output current i_{sabc} to compensate the voltage reference and thereby, achieve a similar effect as the actual reactance in the line.

Then, to satisfy the condition of Eq. (23), the selection law of the virtual impedance should be

$$\frac{J_s}{J_g}=\frac{X'_d+X_{lineg}}{X_f+X_{lines}+X_{vr}} \tag{24}$$

However, it is challenging to accurately measure the inertia. Consider the following expression [21]

$$J_g=\frac{2HS_{ng}}{\omega_n^2} \tag{25}$$

As shown in Eq. (25), the inertia and the inertia time constant H (which generally ranges from 1 s to 10 s) of the DSG are related to its power capacity. Because there is a similar law of the VSG, the inertia matching of the VSG and DSG can be

$$\frac{J_s}{S_s}=\frac{J_g}{S_g} \tag{26}$$

Thus, the virtual inductance can be designed effectively as

$$\frac{S_{ns}}{S_{ng}}=\frac{X'_d+X_{lineg}}{X_f+X_{lines}+X_{vs}} \tag{27}$$

By varying L_{vr}, the equivalent output impedance of the VSG can be varied, and Eq. (23) can be satisfied approximately to eliminate the oscillation generation conditions to the extent feasible.

3.2 Fast oscillation decay principle with dynamic mutual damping

In a practical system, the virtual inductance cannot completely eliminate the oscillation generation conditions. Therefore, the second key concept of the proposed method is the addition of the dynamic mutual damping to further speed up the decay of the oscillation.

The principles of the dynamic mutual damping are shown in the yellow block in Fig. 4. Here, the angular frequency ω_g of the DSG is detected and transferred to the VSG by communication. Subsequently, the difference between ω_g and the output angular frequency ω_s of the VSG is multiplied by the mutual damping coefficient D_{dm} to obtain the dynamic damping torque T_{dm}. Then, T_{dm} would help narrow the output torque difference between the VSG and DSG. Finally, the amplitude and duration of the power oscillation would be reduced, and their output power would tend toward consistency in the minimum time.

After the addition of dynamic mutual damping, the swing equation of VSG becomes

$$T_{ms}-T_{es}-D_{ps}(\omega_n-\omega_s)-D_{dm}(\omega_s-\omega_g)=J_s\dot{\omega}_s \tag{28}$$

It can be observed from Eq. (25) that the dynamic mutual damping becomes effective only when the system is in a dynamic process ($\omega_s \neq \omega_g$). Meanwhile, $\omega_s = \omega_g$ in a steady state, i.e., the mutual damping would become zero. Therefore, it would not affect the system steady-state operation.

It is noteworthy that the addition of mutual damping would also influence the variation ratio of the VSG frequency

$$\Delta\left(\frac{d\omega_s}{dt}\right)=-\frac{D_{dm}(\omega_s-\omega_g)}{J_s} \tag{29}$$

Hence, an excessively large D_{dm} may degrade the system stability. The following is considered to be the design principle of D_{dm}: in a period T, the reduction in the frequency difference between the VSG and DSG caused by the mutual damping should be less than or equal to the difference at the beginning of the period

$$\Delta\left|\frac{d(\omega_s-\omega_g)}{dt}\right|\cdot T\leqslant\omega_s-\omega_g \tag{30}$$

Thereafter, the available range of D_{dm} is

$$0<D_{dm}\leqslant\frac{J_s}{2T} \tag{31}$$

4 Experimental verification

To effectively demonstrate the theoretical analysis and the effectiveness of the proposed method, comparative controller hardware-in-the-loop (CHIL) experiments between the traditional method and proposed method are carried out. The experimental platform is presented in Fig. 6. It consists of the RT-LAB simulator (OP5600), a computer, two control boards (DSP, TMS320F28335), and an oscilloscope. The parameters are shown in Tabs. 2-3. The system topology is shown in Fig. 2. The impedance Z_{lines} and Z_{lineg} are set as (0.1+j0.2) Ω. The local loads are set as follows: $Load_1$=100 kW+50 kVar, and $Load_2$= 150 kW.

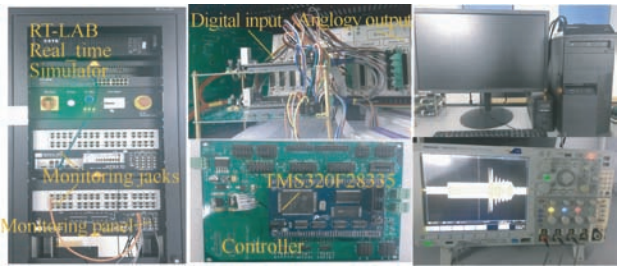

Fig. 6 CHIL experimental platform

Tab. 2 Parameters of VSG

Parameter	Value	Parameter	Value
P_{ns}/kW	50	K	9 200
E_{ns}/V	380	L_f/mH	1.5
D_{ps}/(N • ms/rad)	20	C_f/μF	10
D_{qs}	2 500	L_{vr}/mH	4
J_s/(kg • m^2)	2	D_{dm}	10

Tab. 3 Parameters of DSG

Parameter	Value	Parameter	Value
S_{ng}/(kV • A)	200	X_d^*	1.26
V_{ng}/V	380	X_q^*	1.06
$\tau(s)$	0.6	$X_d'^*$	0.313
p	2	$X_q'^*$	0
H/s	2	D_{pg}/(N • ms/rad)	0.4
T_d'' /s	2.1	K_{pg}/(N • ms/rad)	74

4.1 Performance verification under load fluctuation

This group of experiments verifies the effectiveness of the proposed strategy when the load fluctuates. The idle frequency of the DSG is set as 50.5 Hz. $Load_1$ is activated initially. Meanwhile, $Load_2$ is activated at t=4 s, and cut off at t=12 s. The experimental results of the frequency, power, and current of the VSG and DSG when the conventional method is applied are shown in Fig. 7.

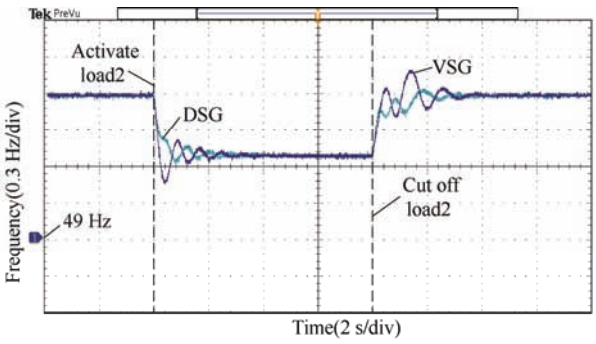

(a) Frequency of VSG and DSG

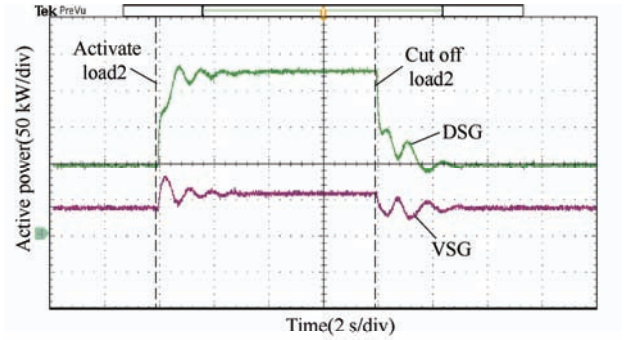

(b) Output active power of VSG and DSG

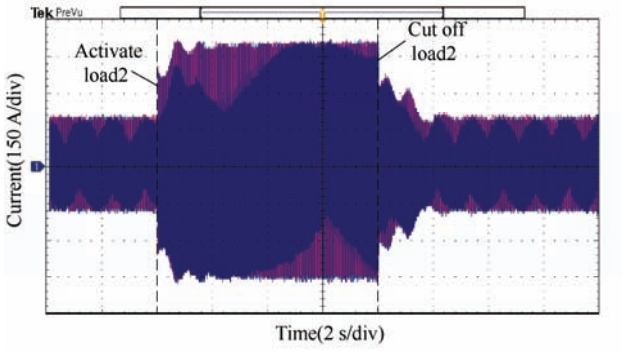

(c) Output current of DSG

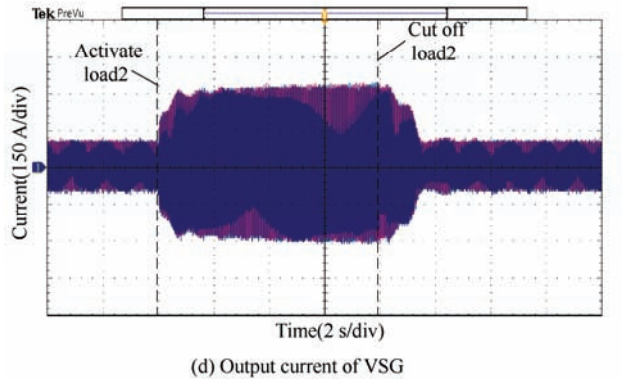

(d) Output current of VSG

Fig. 7 Experimental results without proposed method

As shown in Fig. 7, the frequencies of the VSG and DSG stabilize at 50.2 Hz at the beginning when the conventional method is used. At t=4 s, when $Load_2$ is activated, the frequency and output power of the VSG and DSG present significant instantaneous overshoot and oscillations. It can be observed from Figs. 7a-7b that the reduction in the VSG frequency can be up to 49.3 Hz, and the power overshoot can attain nearly 94 kW. Compared with its steady-state output power (60 kW), the overshoot exceeds 50%. After the inrush stage, the oscillation process of the frequency, power, and output current of the VSG and DSG continues for approximately 3 s. A similar phenomenon occurs when $Load_2$ is removed.

The experimental results of the proposed method are shown in Fig. 8. The virtual inductance L_{vr} is set as 4 mH according to the theoretical analysis. It can be observed that the maximum output power of the VSG in the dynamic process is 74 kW. Compared with the conventional method in Fig. 7, the percentage of power overshoot is reduced from 50% to 20%. The current response is also improved significantly.

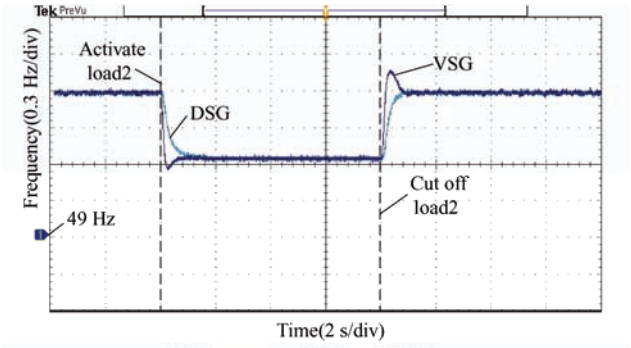

(a) Frequency of VSG and DSG

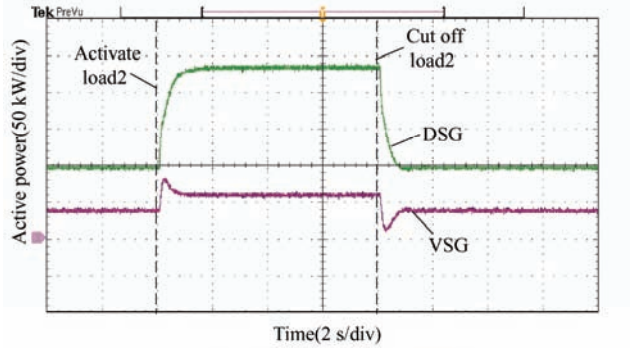

(b) Output active power of VSG and DSG

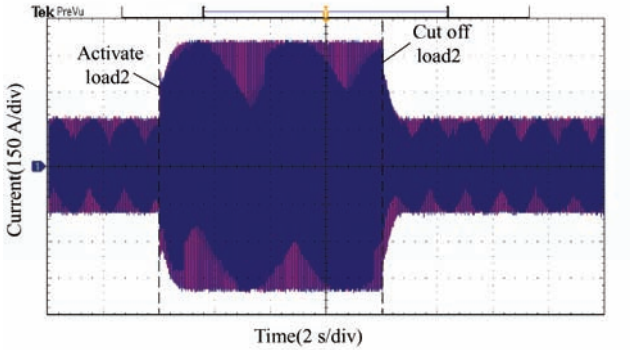

(c) Output current of DSG

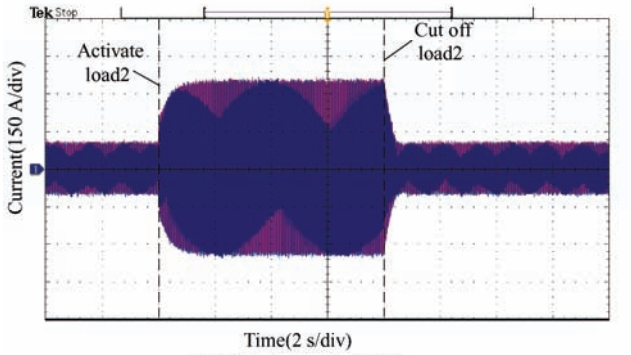

(d) Output current of VSG

Fig. 8 Experimental results with proposed strategy

In addition, the frequency and power of the VSG and DSG can attain their stable states 0.5 s after the load fluctuations. The steady state frequencies are 50.2 Hz and 49.78 Hz, respectively, which are consistent with the outcomes in Fig. 7. This also indicates that the dynamic mutual damping does not affect the system performance in the steady state.

4.2 Performance verification under plug-in and plug-out of VSG

This group of experiments verifies the performance of the proposed strategy under plug-in and plug-out of the VSG or DSG. These experiments are conducted considering that this type of operation is also a common dynamic process of the VSG-DSG paralleled system.

As shown in Fig. 9 and Fig. 10, when the VSG is disconnected from the paralleled system at t=4 s, both VSG and DSG can remain stable regardless of whether

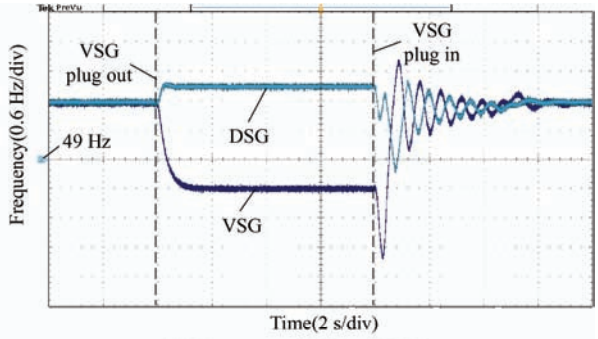

(a) Frequency of VSG and DSG

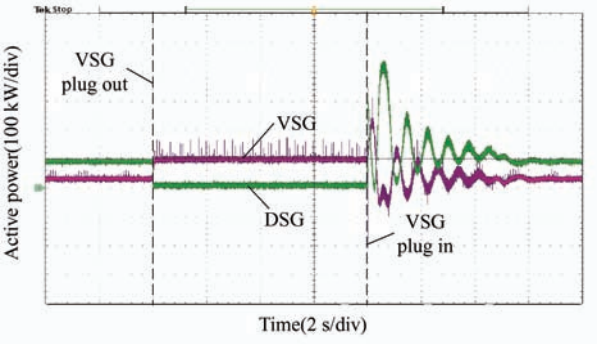

(b) Output active power of VSG and DSG

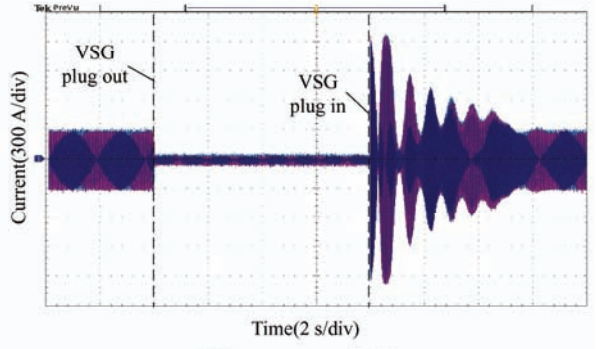

(c) Output current of DSG

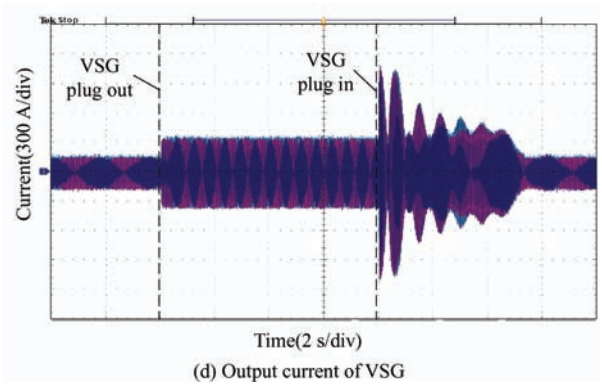

(d) Output current of VSG

Fig. 9 Experimental results under plug-in and plug-out of VSG without proposed method

the proposed method is used or not. Moreover, because both these have voltage and frequency support properties, their local loads can be supplied effectively.

However, when the VSG is re-connected to the DSG at t=12 s, both these sustain severe frequency and power inrush as shown in Figs. 9a-9b. The peak values of the VSG can attain $\pm 5.6\%f_{ns}$ and $\pm 4P_{ns}$, respectively, and those of the DSG can attain $\pm 5.6\%f_{ng}$ and $\pm 2.5P_{ng}$, respectively. Furthermore, their frequencies and power subsequently maintain intense oscillations for a long time. As shown in Fig. 9d, the current of the VSG far exceeds $2I_{ns}$. This would burn the inverter.

As shown in Fig. 10, the frequency and power oscillations can be suppressed rapidly (within 0.5 s) when the proposed method is applied. In addition, smaller frequency and power overshoots occur at the re-connection time. More importantly, as can be observed in Figs. 10c-10d, the current of the VSG and DSG can be always within two times of their rated values. Thus, it is evident that the proposed strategy can also achieve good performance in the case of plug-in and plug-out of a VSG.

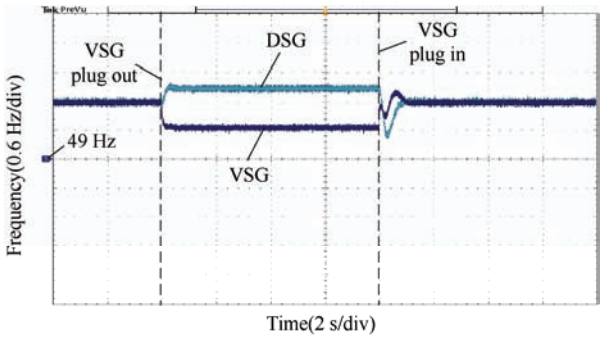

(a) Frequency of VSG and DSG

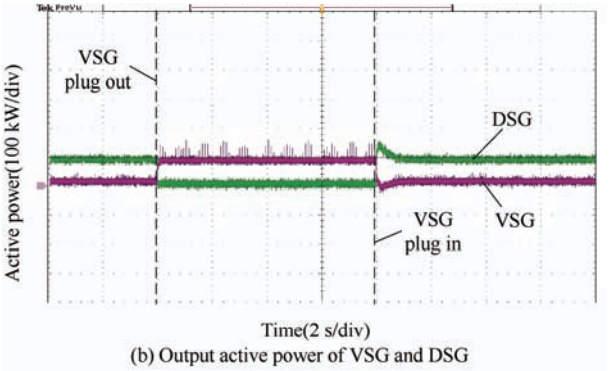

(b) Output active power of VSG and DSG

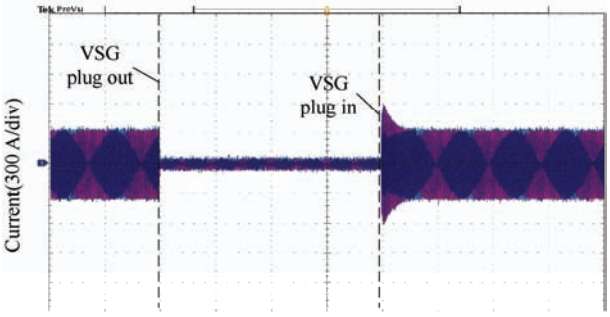

(c) Output current of DSG

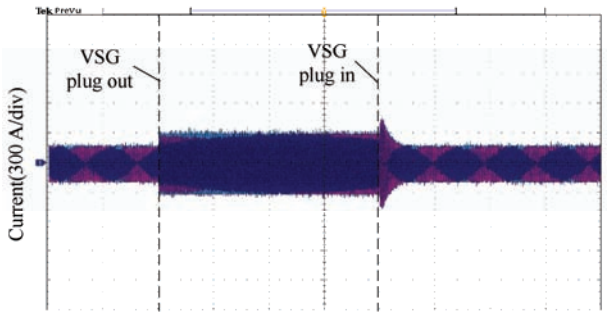

(d) Output current of VSG

Fig. 10 Experimental results under plug-in and plug-out of VSG with proposed strategy

5 Conclusions

This study investigates the interactive power oscillation problem in a VSG-DSG paralleled system when the load fluctuates. The mechanism of the power oscillation is analyzed theoretically. A suppression strategy is proposed based on the analysis results. The conclusions drawn are as follows.

(1) The power oscillation is caused essentially by the physical difference and parameter mismatch between the VSG and DSG. When the inertia of the DSG is significantly higher than that of the VSG, the paralleled system is sensitive only to the parameters of the VSG rather than the DSG. When the inertia of the DSG is similar or significantly smaller than that of the VSG, the system is sensitive to all parameters and is

more likely to oscillate. In both the scenarios, the equivalent impedance has a significant impact on the oscillation frequency.

(2) Although the VSG and DSG differ in their physical structure, the elimination conditions of the interactive power oscillation generation can be satisfied when the equivalent impedance of the VSG and DSG are inversely proportional to their capacities (assuming that their inertia are proportional to the capacities).

(3) With the proposed suppression strategy, the virtual inductance is designed and added to the VSG to approximately eliminate the condition for oscillation generation. Meanwhile, the dynamic mutual damping is dedicated to the reduction of the output torque difference between the VSG and DSG when the load fluctuates, and the acceleration of the oscillation decay.

References

[1] J Liu, Y Miura, T Ise. Comparison of dynamic characteristics between virtual synchronous generator and droop control in inverter-based distributed generators. *IEEE Transactions on Power Electronics*, 2015, 31(5): 3600-3611.

[2] Q Zhong, G Weiss. Synchronverters inverters that mimic synchronous generators. *IEEE Transactions on Industrial Electronics*, 2011, 58(4): 1259-1267.

[3] X Xi, H Geng, G Yang, et al. Torsional oscillation damping control for DFIG-based wind farm participating in power system frequency regulation. *IEEE Transactions on Industry Applications*, 2018, 54(4): 3687-3701.

[4] Y Shao, C Zhu, S Dong, et al. Adaptive damping coefficient control of virtual synchronous generator of microgrid inverter. *2019 29th Australasian Universities Power Engineering Conference (AUPEC)*, 2019.

[5] Z Shuai, C Shen, X Liu, et al. Transient angle stability of virtual synchronous generators using Lyapunov's direct method. *IEEE Transactions on Smart Grid*, 2019, 10(4): 4648-4661.

[6] Y Zhu, M Peng, X Yu, Research on improved virtual synchronous generator based on differential compensation link. *2018 IEEE 3rd International Conference on Integrated Circuits and Microsystems (ICICM)*, Shanghai, 2018: 259-263.

[7] R J Nikam, R R Purkar. Oscillation damping reduction methodology for distributed generator using VSG. *2018 International Conference on Smart Electric Drives and Power System (ICSEDPS)*, 2018: 126-131.

[8] H Wu, X Ruan, D Yang, et al. Small-signal modeling and parameters design for virtual synchronous generators. *IEEE Transactions on Industrial Electronics*, 2016, 63(7): 4292-4303.

[9] N Soni, S Doolla, M C Chandorkar. Inertia design methods for islanded microgrids having static and rotating energy sources. *IEEE Transactions on Industry Applications*, 2016, 52(11): 5165-5174.

[10] J Liu, Y Miura, H Bevrani, et al. Enhanced virtual synchronous generator control for parallel inverters in microgrids. *IEEE Transactions on Smart Grid*, 2017, 8(5): 2268-2277.

[11] Z Shuai, W Huang, J Shen, et al. Active power oscillation and suppression techniques between two parallel synchronverters during load fluctuations. *IEEE Transactions on Power Electronics*, 2020, 35(4): 4127-4142.

[12] H Cheng, Z Shuai, C Shen, et al. Transient angle stability of paralleled synchronous and virtual synchronous generators in islanded microgrids. *IEEE Transactions on Power Electronics*, 2020, 35(8): 8751-8765.

[13] X Zhang, L Fu, F Ma, et al. An emergency control strategy for isolated power system of three-phase inverter and diesel-engine generator operating in parallel. *IEEE Access*, 2018(6): 66223-66234.

[14] K Shi, W Song, H Ge, et al. Transient analysis of microgrids with parallel synchronous generators and virtual synchronous generators. *IEEE Transactions on Energy Conversion*, 2020, 35(1): 95-105.

[15] K Lin, F Xiao, G Jie, et al. Control strategy for inverter parallel and parallel with synchronous generator based on virtual synchronous generator theory. *2017 36th Chinese Control Conference (CCC)*, Dalian, 2017: 6453-6459.

[16] R Shi, X Zhang, L Fang, et al. Research on power compensation strategy for diesel generator system based on virtual synchronous generator. *2016 IEEE 8th International Power Electronics and Motion Control Conference (IPEMC-ECCE Asia)*, Hefei, 2016: 939-943.

[17] Y Wang, J Meng, X Zhang, et al. Control of PMSG-based wind turbines for system inertial response and power oscillation damping. *IEEE Transactions on Sustainable Energy*, 2015, 6(2): 565-574.

[18] Fei Li, Canbing Li, Kai Sun, et al. Capacity configuration of hybrid CSP/PV plant for economical application of solar energy. *Chinese Journal of Electrical Engineering*, 2020, 6(2): 19-29.

[19] Liang Chen, Heng Nian, Yunyang Xu. Improved model predictive direct power control of grid side converter in weak grid using Kalman filter and DSOGI. *Chinese Journal of Electrical Engineering*, 2019, 5(4): 22-32.

[20] Z Shuai, Y Peng, X Liu, et al. Dynamic equivalent modeling for multi-microgrid based on structure preservation method. *IEEE Transactions on Smart Grid*, 2019, 10(4): 3929-3942.

[21] P Kundur. Power system stability and control. 1st ed. Canada: Mcgraw-Hill, 2001.

Zhiyong Yuan received his Ph.D. degree in Electrical Engineering from Tsinghua University, in 2006. He is currently the Director of Power Distribution Network Department, Electric Power Research Institute, China Southern Power Grid Co., Ltd. His research interests include power electronics and microgrids.

Xia Shen received the B.S. degree in Electrical Engineering from Jiangsu University, Zhenjiang, China, in 2016. Now she is currently working toward the Ph.D degree in Power Electronics in the College of Electrical Engineering at Hunan University, Changsha, China. Her research interests include fault analysis and control of hybrid AC/DC microgrid.

Yingjie Tan received the Ph.D. degree in Electrical Engineering from the University of Wollongong, Wollongong, NSW, Australia, in 2017. He is currently a Research Fellow with Electric Power Research Institute, Guangzhou, China Southern Power Grid Co., Ltd. His research interests include power electronics, renewable distributed generation and microgrids.

Zhenhua Tan received the undergraduate degree in Electrical Engineering from the Hunan University, China, in 2019. He is currently studying in Hunan University as a master's degree student. His research interests are artificial intelligence and microgrid technology.

Jinyong Lei received his B.S. and Ph.D. degrees in Electric Engineering from the Department of Electrical Engineering, Zhejiang University, Zhejiang, China, in 2005 and 2010, respectively. Currently, he is the Principle Engineer with the Power Distribution Network Department, Electric Power Research Institute, China Southern Power Grid Co., Ltd. His research interests include distributed generation, renewable energy and microgrid.